Journal of Alloys and Compounds 508 (2010) 446–452

Contents lists available at ScienceDirect

Journal of Alloys and Compounds

journal homepage: www.elsevier.com/locate/jallcom

Frictional shear induced modification of the mechanical properties of TiAl(Nb) intermetallics near the surface

N. Deyneka-Dupriez [a], A.P.M. Iqbal [a], S. Das [b,*], R. Wunderlich [a], H.-J. Fecht [a]

[a] Institute of Micro- und Nanomaterials, Ulm University, D-89081 Ulm, Germany
[b] Department of Metallurgical and Materials Engineering, Indian Institute of Technology, Kharagpur 721 302, India

ARTICLE INFO

Article history:
Received 19 January 2010
Received in revised form 14 August 2010
Accepted 24 August 2010
Available online 19 September 2010

Keywords:
Titanium aluminide
Polishing
Hardening
Nanomechanical testing

ABSTRACT

Mechanical properties of the two-phase TiAl(Nb) alloys have been studied after being subjected to mechanical as well as electrolytic polishing. Indentation tests at different maximum loads using different instrumentation allow probing the overall mechanical behavior of the alloys. Nanoindentation experiments have been carried out to study the local hardening of each phase during mechanical polishing. Since the deformation of γ-TiAl is facilitated by twin formation, the mechanical polishing associated with considerable frictional forces causes a significant work hardening of the γ-TiAl phase resulting in an enhancement of the overall surface hardness of the alloy. A similar hardening effect has been observed during a scratch test. The influence of local hardening owing to different crystal structures on the overall mechanical behavior in the mechanically polished alloys has also been investigated.

1. Introduction

In engineering applications, such as turbine blade materials, various mechanical properties of the titanium aluminides must be well balanced. The mechanical properties of titanium alloys are predominantly determined by the chemical composition as well as the corresponding microstructure [1–11]. Therefore, a detailed characterization of titanium aluminides (Ti–Al) is essential in order to understand the link between the processing, microstructure and mechanical performance, with a focus on the meso- to nanoscale.

The lamellar structure of the $(\alpha_2 + \gamma)$ two-phase Ti–Al alloys has been developed as a promising structure because of its good fracture toughness and creep properties [12]. Since the integral mechanical property of any material originates from the mechanical properties of all the component phases and their distribution, the testing of the mechanical property of each phase is of significant importance for the understanding as well as controlling the mechanical behavior of the bulk material.

The bulk mechanical properties of the intermetallic TiAl alloy, correlated with the microstructure and also different strengthening effects, have been extensively studied by many authors [1–11]. Appel et al. [13] have reported the deformation mechanism of such alloys. Research work has been carried out to examine the mechanical properties of this alloy on a nanometer scale [1,14–16]. A nanoindenting atomic force microscope has been used to determine the hardness and modulus of Ti–45Al–4.6Nb–0.2B–0.2C and Ti–45Al–1Cr alloys with different microstructures [14] as well as of different lamellae and domains in polysynthetically twinned TiAl [15,16]. Cao et al. have reported the nanoindentation results on the carbides in Ti–46.6Al–1.45C alloy [1]. They observed that both hardness and modulus increased at the vicinity of the carbides and discussed the role of carbides on the mechanical properties of the alloy.

The tribological behavior of the bulk TiAl alloys have also been studied and reported elsewhere [17–20]. However, the properties of most tribo-mechanical systems may change during the functional performance of the system owing to the tribological process. One of the possibilities of tribo-induced changes of interacting but moving surfaces is an increase in the strength as a consequence of the effects like “strain hardening” due to the contact stresses and the generation of internal stress fields. In mechanical engineering, this aspect is quite important and should be considered in the design of the tribological system. A change in the material hardness leads to the changes in the plastic contact deformation and wear process during sliding resulting in the modification of the surface topography. The changes in the surface topography influence the functional behavior of the whole tribo-mechanical system with respect to the limits of lubrication or running-in effect [21]. Recently, Kouhanjani et al. showed that in the case of the Cu–Cr alloy a prior cold working led to an increase in hardness and wear rate of this alloy [22].

According to Bowden and Tabor [23], during mechanical polishing of the metals the surface flow may occur owing to frictional force as well as heating caused by frictional force. The amount of

* Corresponding author. Tel.: +91 3222 283256; fax: +91 3222 220666.
E-mail address: sdas.iitkgp@gmail.com (S. Das).

0925-8388/$ – see front matter © 2010 Elsevier B.V. All rights reserved.
doi:10.1016/j.jallcom.2010.08.091

surface flow depends on the relative mechanical properties of the solid. The mechanical polishing, however, leads to the formation of the strain-hardened sub-surface layer [24], which may improve fatigue strength of the Ti–Al alloy [25]. The electrolytic polishing is chosen to remove this highly deformed and partly fractured layer. Both the mechanically and electrolytic polished surfaces of the Ti–46Al–8Nb two-phase alloys with a near fully lamellar microstructure are investigated here. The indentation hardness of the materials, as a markedly “structure-dependent property”, is mainly considered to be the most relevant to characterize the tribo-induced surface strength changes on micro- as well as nanoscale [25]. The nanoindentation experiments have also been carried out to establish also the individual role of the constituent phases with the aim of correlating the local near-surface mechanical properties with the overall mechanical behavior of the system. The scratch test results confirm the surface strengthening effect.

2. Experimental

Samples of Ti–46Al–8Nb and Ti–46Al–8Nb–0.2C alloys after centrifugal casting and hot-isostatic pressing (240 min at 1260 °C and 200 MPa) were received from ACCESS (Aachen, Germany). The mechanical polishing procedure adopted for the alloys under investigation is as follows: the first stage is the wet grinding on SiC-papers ranging from grit 400 to 4000 with a moderate pressure on the disk. Then further polishing has been achieved with the colloidal silicon dioxide of 0.04 μm grit size on a synthetic leather cloth mounted disk rotating at 1500 rpm. The selected samples have been electrolytic polished in a Buehler Polimat 2 system for 15 s with a voltage of 35 V. The electrolyte used is a mixture of methanol, 2-butoxy-ethanol and perchloric acid procured from Fa. Struer's.

The alloys studied here are based on the γ-TiAl intermetallic phase and it also contains a second phase, α_2-Ti_3Al. The micromechanical testing has been carried out using a Vickers hardness tester (Buehler) performing 10 indents and Nanoindenter XP (MTS Nano Instruments) performing 30 indents. A load of 500 mN is applied. Hysitron TriboScope is used for the nanomechanical testing: nanoindentation and nanoscratching. It is a quantitative depth-sensing nanoindenter which tests surfaces yielding property with a high spatial resolution $\Delta d = 0.5$ nm and highly controlled quantitative forces $\Delta F = 2.5$ μN. The samples are indented using a maximum load of 3 mN, so that each phase of the alloy could be tested separately and the indentation could be easily found afterwards during the scanning electron microscopy (SEM). Matrixes of 100 indents are performed. In the nanoscratching process, a constant, normal force of 500 μN is applied by pressing a diamond tip on the specimen surface. Simultaneously, a lateral displacement is introduced and the tip is moving back and forth 10 times scratching the surface over the length of 4 μm. A lateral force and normal displacement of the tip are measured.

For the indentation with both the Nanoindenter and Hysitron TriboScope, a three-sided pyramidal Bekovich diamond tip with a total opening angle of 142.5° is used. The indentations are performed with a loading duration of 15 s. The applied load and penetration depth data are recorded and analyzed by the Oliver–Pharr method [26] to obtain the hardness and reduced modulus of the sample. Young's modulus of the tested material is calculated from the reduced modulus using the measured value of the Poisson's ratio.

For the evaluation of Poisson's ratio, the ultrasonic testing system consisting of the ultrasonic impulse generator (Krautkramer-Branson USIP12), oscilloscope and Panametrics-NDT Ultrasonic longitudinal and shear contact transducers has been used. The longitudinal and shear wave speed in the material are measured. The transit time of ultrasonic waves in the material has been determined in the pulse echo (PE) mode with a frequency of 5 MHz.

The in situ imaging facility of Hysitron TriboScope interfaced with the multimode DI 3100 Atomic Force Microscope (AFM) records a three-dimensional image of the tested area. In order to visualize the phases and to identify individual indent site, the sample areas with the matrixes of indents are characterized with the help of a high resolution Leo 1550 SEM in the back-scattered electron (BSE) mode.

3. Results and discussion

3.1. Mechanical properties of alloys on micro- and nanoscale after different surface treatment

Table 1 compares the average Vickers hardness (*HV*) and micro-hardness (*H*) of the Ti–46Al–8Nb and Ti–46Al–8Nb–0.2C alloys, obtained by using the Vickers hardness tester and nanoindenter, respectively. Vickers hardness values can be compared with those obtained recently for the Ti_2AlC/TiAl composite sintered at 750 °C [3] and for directionally solidified Ti–46Al–0.5W–0.5Si alloy with a large dendritic spacing [4].

The results of the nanomechanical testing with Hysitron TriboScope are also presented in Table 1 as the crossed average values of nano-hardness (*H*) and Young's Modulus (*E*). These results show that the alloy containing carbon is harder and has slightly higher elastic modulus compared to the alloy without carbon (except the nano-hardness of the mechanically polished samples). The role of the carbon in the deformation process of two-phase TiAl alloys has been already discussed elsewhere [13,27]. The short range interaction of the dissolved carbon with the dislocations may result in a solid solution hardening [27] of the electrolytically polished Ti–46Al–8Nb–0.2C alloy.

The measured Young's modulus of both alloys is in agreement with the results of the nanoindentation measurements performed by Kempf et al. on the polysynthetically twinned PTS-TiAl using a conical tip at 1 mN or a cube-corner tip at 0.8 mN [16]. However, this is lower than that one (180–200 GPa) obtained by Göken et al. using the Berkovich tip at 1 mN [15]. Since no pronounced pile-up behavior of the indentation has been observed, the difference of *E* from those reported by Göken et al. may be attributed to the different composition and stress state in the alloys which are known to influence the nanoindentation measurements [15].

Table 1 demonstrates that for both mechanically polished samples the nano-hardness is higher than the micro-hardness obtained by nanoindentation and Vickers hardness testing, respectively. This can be attributed to the fact that the nanomechanical testing reveals the properties of sub-surface layer; in this case it is the strain hardened (or cold worked) layer. The thick surface cold working layer containing non-equilibrium concentration of point defects is known to be formed as a result of certain pressure and deformation during mechanical polishing [24] of the γ-TiAl alloys [13,27]. The very high defect density in the cold-worked surface layer is nearly unaffected by the additional dislocation density required to form the residual impression during the nanoindentation [24] resulting in a higher measured value of hardness at the surface.

It can be speculated here that the surface modification of the intermetallic alloys/compounds are different compared to that of the conventional structural materials. The plastic deformation of the titanium aluminides in the near-surface region caused by the frictional force may result in the formation of nanostructure in this near-surface region. This may change the mechanical properties significantly. This behavior is quite similar to that generally observed in some steels and nickel-based superalloys after surface grinding.

The cold-worked layer generated during mechanical polishing has been removed by electrolytic polishing; the nano-hardness measured at the surface of both electrolytic polished alloys approximates the Vickers hardness (Table 1). Thus, the measured hardness data, listed in Table 1, is probably insignificantly affected by an intrinsic surface property (known as indentation size effect). The values, obtained on electrolytic polished samples, can be related to the bulk hardness of these alloys.

In order to show the change in hardness with the depth, in Fig. 1 the hardness values from Table 1 are plotted as a function of the maximum indenter penetration depth (typical conversion of the Berkovich hardness *H* into Vickers hardness: $HV = 94.59H$ [28]). The indentation depths for the load of 500 mN in the case of nanoindenter and Vickers hardness tester are ~2.3–2.5 μm and ~3.5–3.7 μm, respectively. Whereas, the penetration depth with a load of 3 mN using the Hysitron TriboScope is only ~135 nm. The difference in the maximum penetration depths at the same load of nanoindentation and Vickers testing techniques is related to the different indenter geometry.

When the mechanically polished alloys are compared in Fig. 1, it appears that the surface hardness of the Ti–46Al–8Nb–0.2C alloy is

Table 1
Crossed average values of hardness measured with different instrumentation; Young's modulus and Poisson's ratio of Ti–46Al–8Nb and Ti–46Al–8Nb–0.2C alloys with differently treated surfaces.

	Ti–46Al–8Nb		Ti–46Al–8Nb–0.2C	
	Mechanically polished	Electrolytic polished	Mechanically polished	Electrolytic polished
Vickers hardness, *HV*	370.9 ± 21	361.32 ± 19	399.2 ± 30	400.03 ± 13
Micro-hardness, *H* (GPa) (NanoIndenter XP)	4.0 ± 0.4		4.5 ± 0.2	
Nano-hardness, *H* (GPa) (Hysitron TriboScope)	5.5 ± 0.7	3.6 ± 0.5	5.0 ± 0.9	4.1 ± 0.5
Young's modulus, *E* (GPa) (Hysitron TriboScope)	161.1 ± 13	155.5 ± 11	167.4 ± 13	161.0 ± 10
Poisson's ratio ν	0.27 ± 0.023		0.279 ± 0.011	

lower than that of the Ti–46Al–8Nb alloy. Fig. 1 also demonstrates that the difference between the surface hardness values of mechanically and electrolytic polished specimens of the Ti–46Al–8Nb–0.2C alloy is lower than that of the Ti–46Al–8Nb alloy. However, at a depth of 2.5 μm this difference becomes similar for both the alloys. The hardening effect at the surface of the Ti–46Al–8Nb–0.2C alloy may be reduced by the presence of carbon; carbon may play a hindering role in the deformation caused by the ordinary dislocations and twinning during mechanical polishing leading to the lower amount of near-surface cold work (dislocation density).

Nanomechanical testing of constituent phases, structural features and harderning was mostly adverted to Ti–46Al–8Nb alloy. For Ti–46Al–8Nb–0.2C alloy similar behavior was observed.

3.2. Effect of polishing on hardness of constituent phases

Phase resolved indentation using the Hysitron TriboScope has been performed on both alloys with different surface preparations. Fig. 2(a) shows the microstructure of the electrolytically polished Ti–46Al–8Nb alloy along with the indentation mark. Owing to a higher amount of Ti, the α_2 phase appears to be brighter than the γ phase containing less amounted Ti in the SEM micrograph obtained in the BSE mode. Since, the α_2 phase dissolves faster than the γ phase during electrolytic polishing, the topographic height contrast can be obtained in an AFM, Fig. 2(b). The indentation on γ- and α_2-phases are marked in Fig. 2(a) and (b) and corresponding load–displacement curves are highlighted in Fig. 2(c), representing a clear difference in the displacement, i.e., the difference in the hardness, of each phase. The loading curves are punctuated by the discontinuities or 'pop-ins' in which the displacement increases at an approximately constant load. In the crystalline materials the presence of the pop-ins is invariably associated with a discrete plastic deformation phenomenon, such as dislocation nucleation or cracking [29,30].

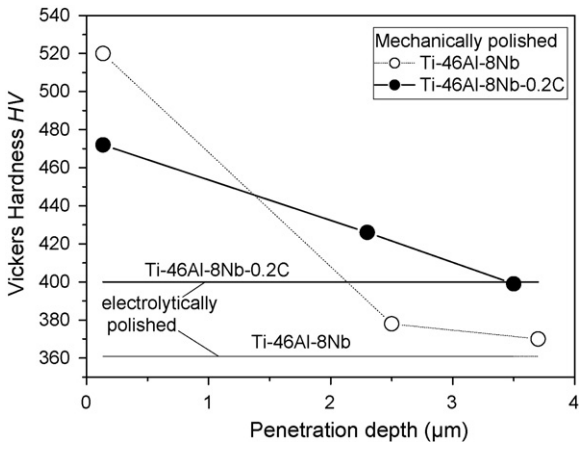

Fig. 1. Dependence of the overall hardness on the penetration depth of the indenter for the mechanically polished Ti–46Al–8Nb (open symbols) and Ti–46Al–8Nb–0.2C (full symbols) alloys. Horizontal lines represent the hardness measured on electrolytically polished samples: dotted line is for Ti–46Al–8Nb alloy and the solid line is for Ti–46Al–8Nb–0.2C alloy.

The results from the indentation measurements, Fig. 2(b), reveal that the α_2 phase with a hexagonal structure is naturally harder (H_α = 5.5 GPa) than the γ phase (H_γ = 3.63 GPa) having a tetragonal structure. However, these values are lower than those earlier reported by Kempf et al. [16] for the α_2 lamellae (7.4 GPa) and γ lamellae (5.2 GPa) in the PTS-TiAl. The direct comparison with the absolute hardness values published in the literature is difficult owing to many factors like microstructure, composition, stresses, pop-ins, etc. These may influence the hardness results.

Fig. 3(a) illustrates the SEM-BSE micrograph with the indentation performed on different phases of the mechanically polished Ti–46Al–8Nb alloy. When examining the topography by an AFM (Fig. 3(b)) together with the SEM imaging in the BSE mode (Fig. 3(a)), it can be seen that the α_2 phase is relatively easy to remove by mechanical polishing, even though hexagonal metals in general exhibit a lower wear characteristic than the cubic metals, and it is related to different plastic asperity contact deformation mode and the number of operable slip systems in the crystal [21]. Fig. 3(b) indicates the softness of the α_2 phase as compared to the γ phase. Nanoindentation curves in Fig. 3(c) shows that the displacement into the surface of α_2 phase is higher than that in the γ phase. Therefore, the hardness value deduced from load–displacement curve recorded during indentation in α_2 phase is lower (H_α = 4.44 GPa) as compared to the hardness of γ phase (H_γ = 5.24 GPa). This is in contrary to the results obtained for electrolytic polished samples (Fig. 2(c)). The reason why tetragonal γ phase after mechanical polishing appears to be harder than α_2 phase with hexagonal structure can be explained as following. The crystals or lamellas of the α_2 phase are difficult to deform, whereas deformation in the γ phase is easily provided by the ordinary dislocations and mechanical twinning. Kempf et al. reported that no significant hardness difference could be deduced for the twinned and untwinned γ-TiAl lamellae [16]. However, at high strain rates the twinning becomes a 'self-stopping' process that may restrict the plastic flow of the intermetallic [31]. Therefore, it is expected that a further deformation of the twinned γ lamellae by the indentation is more difficult, and therefore it results in a higher hardness than that of the α_2 lamellae.

Moreover, owing to lowered relaxation ability of the intermetallic phases caused by the high value of the resistance to the dislocations moving at a high strain rate, the twinning may induce the opening of the brittle micro-cracks in the γ-TiAl [31]. Indeed, a close examination of the SEM-BSE micrograph (Fig. 3(a)) reveals that the mechanical polishing has produced ordered twinning and cracks in the γ-TiAl phase almost throughout the whole sample surface. Both equiaxed grains and lamellar structures are affected. The cracks along the boundaries of equiaxed grains and lamellae can be observed in Fig. 3(a). The grain and lamellar boundaries are the barriers for the propagation of the highly localized strain caused by the mechanical twinning [32,33]. Local stresses near the grain boundaries can be 20–30% higher than the average stress in the material, which may enhance the micro-cracking in the presence

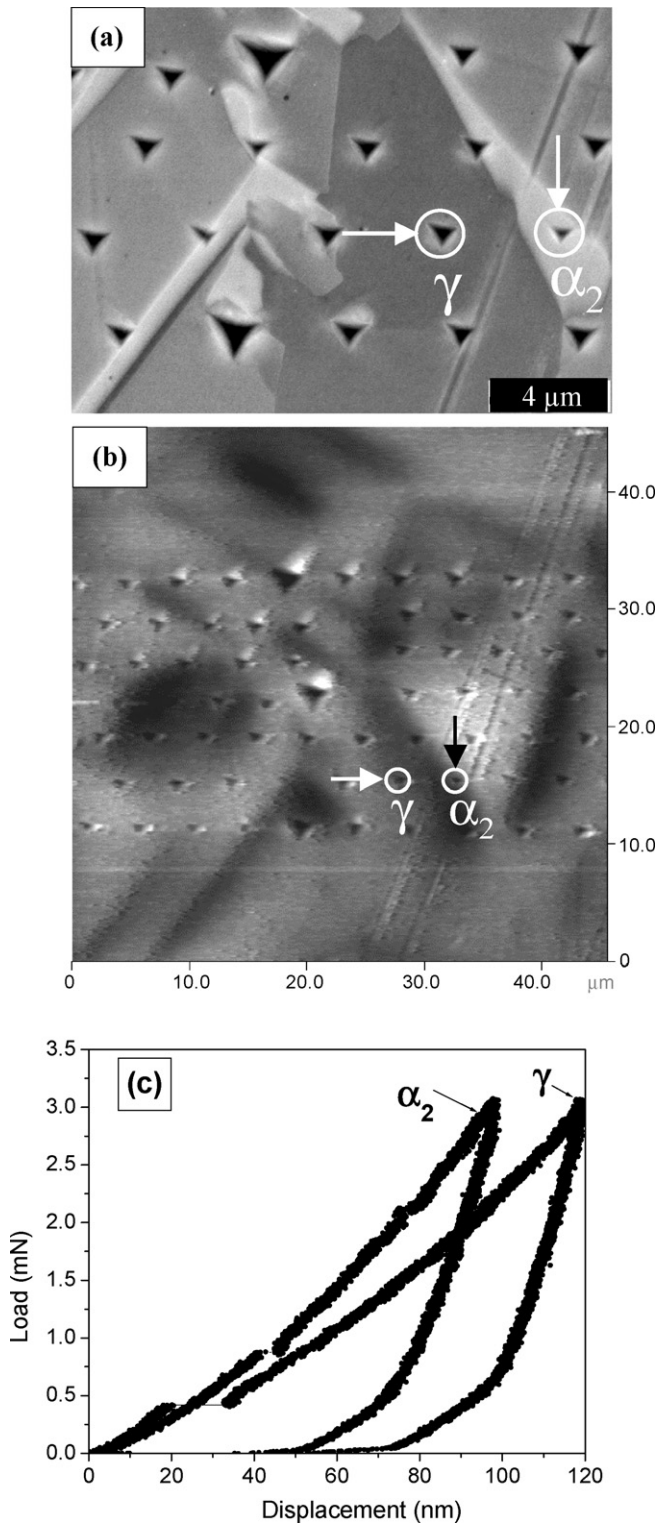

Fig. 2. (a) Scanning electron micrographs (BSE mode) of an array of indents and (b) atomic force microscopy image made on the same area of the electrolytically polished Ti–46Al–8Nb alloy. The scale in the AFM image corresponds to the height difference of 220 nm. (c) Load–displacement curves corresponding to the residual indents from the nanoindentation in the γ- and α_2-phases marked with circles and arrows, respectively.

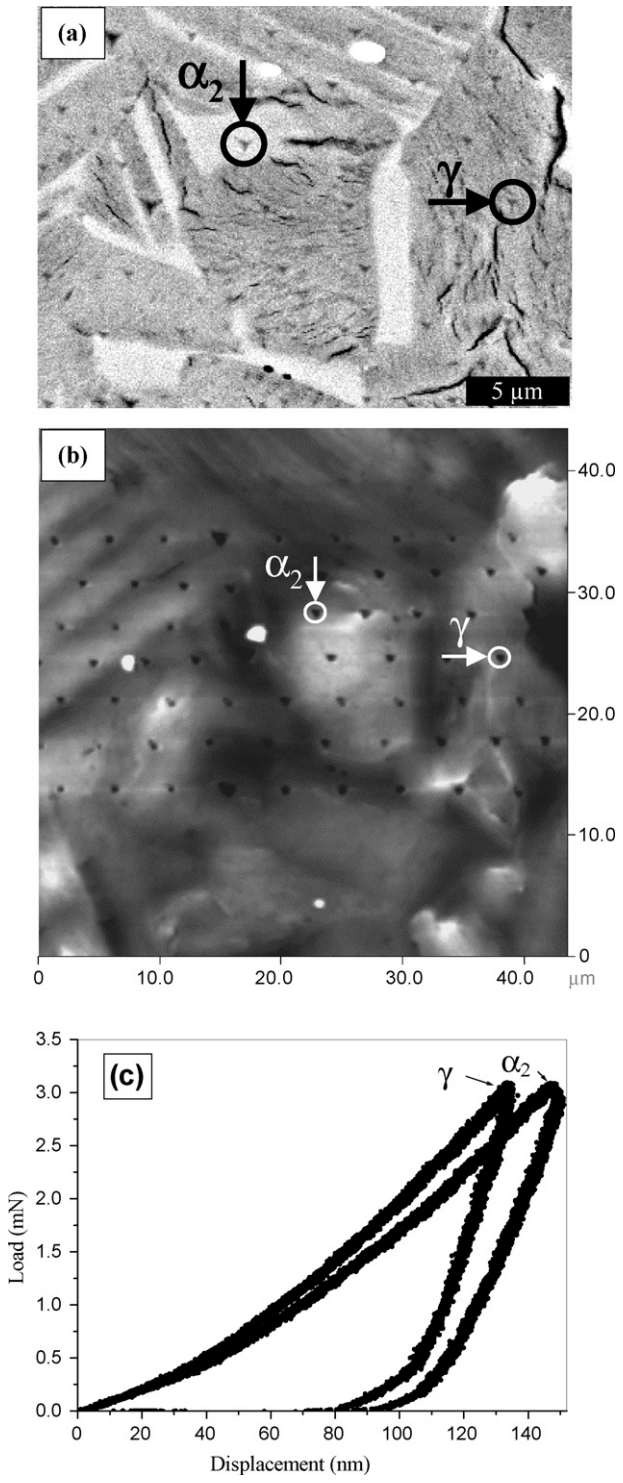

Fig. 3. (a) Scanning electron micrographs (BSE mode) of an array of indents, (b) atomic force microscopy on the same area of mechanically polished Ti–46Al–8Nb alloy. The scale in AFM image corresponds to the height difference of 111 nm. (c) Load–displacement curves corresponding to the residual indents from nanoindentation in the γ- and α_2-phases marked with circles and arrows, respectively.

of other deformation defects. The weak boundaries are especially susceptible to cracking [33].

Following inference may be drawn for both the alloys studied here. Once the overall hardness of the composite is generally assumed to be directly proportional to the hardness of the different constituent phases, and the percentage of the α_2 phase in these alloys is known to be small (10–15%), then nano-hardness is mostly

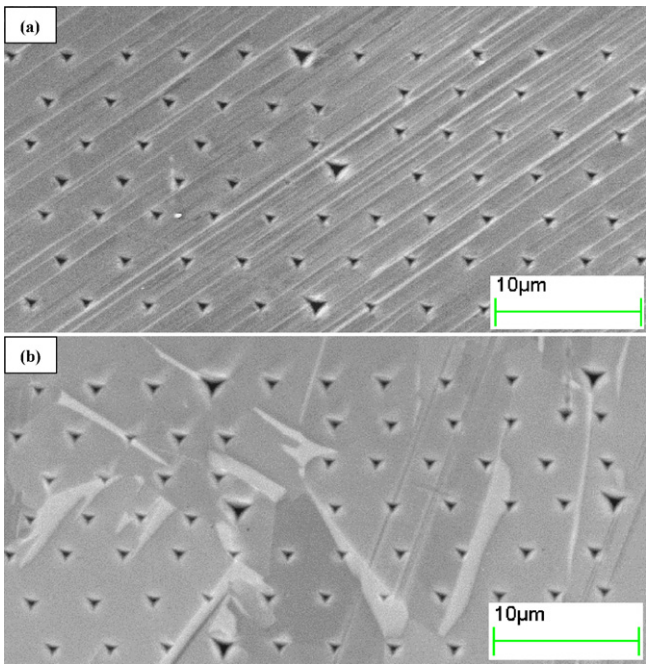

Fig. 4. Scanning electron micrographs (BSE mode) showing microstructure and also arrays of indents (a) on lamellar colony and (b) on equiaxed grains of electrolytic polished Ti–46Al–8Nb alloy.

determined by the hardness of the γ-phase; the surface hardening during mechanical polishing can be correlated with the local hardening of the γ-phase.

3.3. Nanomechanical characterization of different structural features

Near fully lamellar microstructures with a fraction of lamellar constituent 80–90 vol.%, coarse colony structure and the equiaxed grains along the colony boundaries are characteristics for the studied alloys.

The Hysitron TriboScope instrumentation was used to study separately the strengthening of alloys' micro-structural features like lamellar colonies and equiaxed grains. Fig. 4 represents two indentation matrixes performed on the lamellar structure of an electrolytically polished sample (Fig. 4(a)) with an average hardness of 3.8 GPa and on the structure with the equiaxed grains (Fig. 4(b)) with an average hardness of 3.5 GPa.

Fig. 5(a) shows the indents performed on fine lamellar structure and equiaxed γ grains of the Ti–46Al–8Nb alloy. Fig. 5(b) represents the corresponding load–displacement curves. The equiaxed γ grains demonstrate lower hardness as compared to the fine lamellae and the loading curve is punctuated by a pop-in. No pop-ins can be observed on load curve for the fine lamellas. By indenting the fine lamellae, both phases are simultaneously indented. Therefore, the hardness of the fine lamellae is higher than the hardness of the equiaxed grains. However, the plastic deformation in fine lamellae is hindered by the dislocation pile-up at the lamellas boundaries. Lamellar interfaces are known to be the effective glide obstacles for the twinning partial and ordinary dislocations. Thus, the regions with fine lamellar structure are naturally harder according to the Hall–Petch relationship [34] than the regions with the large equiaxed γ grains.

As for the mechanically polished Ti–46Al–8Nb alloy, average hardness value of the equiaxed grains is measured to be 5.7 GPa, and it does not significantly differ from that of the colonies with the lamellar structure having hardness of 5.6 GPa. The corresponding microstructures with the indentation matrixes are shown in Fig. 6. The preferential hardening of the γ phase caused by the mechanical polishing may result in an increase in the average hardness of the equiaxed grains.

In spite of presence of the lamellas boundaries, hardness of the fine lamellar colonies of both electrolytic and mechanically polished samples is not significantly higher than that of the equiaxed grains. This may be due to the surface roughness which may cause a possible lowering of the measured hardness value [35]. Since, the α_2 phase is comparatively easy to remove by the mechanical and electrolytic polishing techniques, the peeks and deep valleys with the lateral size of the single lamella are produced during sample preparation. The near-surface region with a fine lamellar structure is characterized by a greater number of deep valleys per unit areas as compared to the near-surface region with the equiaxed grains. Thus, during an initial indentation stage in fine lamellar structure, the dislocations may escape at the sides of the surface peaks resulting the lowering of average hardness value of such structures.

3.4. Hardening during scratch test

The results of the scratch test performed on electrolytic polished sample of the Ti–46Al–8Nb alloy presented as a difference in the normal tip displacement Δd_n versus the number of scratching cycles is presented in Fig. 7. During first two cycles, Δd_n significantly decreased, i.e., the tip was penetrating the sample surface deeper and deeper. This indicates that at the initial stages of scratching a severe wear occurred. It was followed by a relatively stable behavior of the system under the action of the tribological process (lateral tip movement) which is characterized by a constancy of the difference in penetration depth per cycle (unit time). This can be attributed to the surface hardening beneath the scratching indenter, and it can be compared to some extent to the work hardening occurring during mechanical polishing. A similar effect

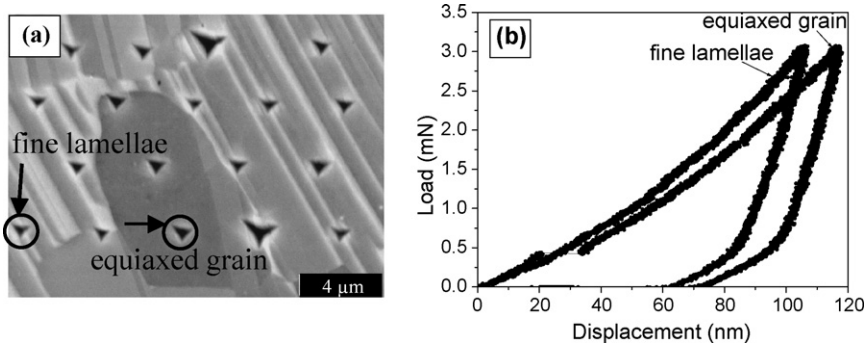

Fig. 5. (a) Scanning electron micrographs (BSE mode) showing microstructure and also arrays of indents on lamellar colony and on equiaxed grains of electrolytic polished Ti–46Al–8Nb alloy. (b) Load–displacement curves corresponding to the residual indents marked with circles and arrows.

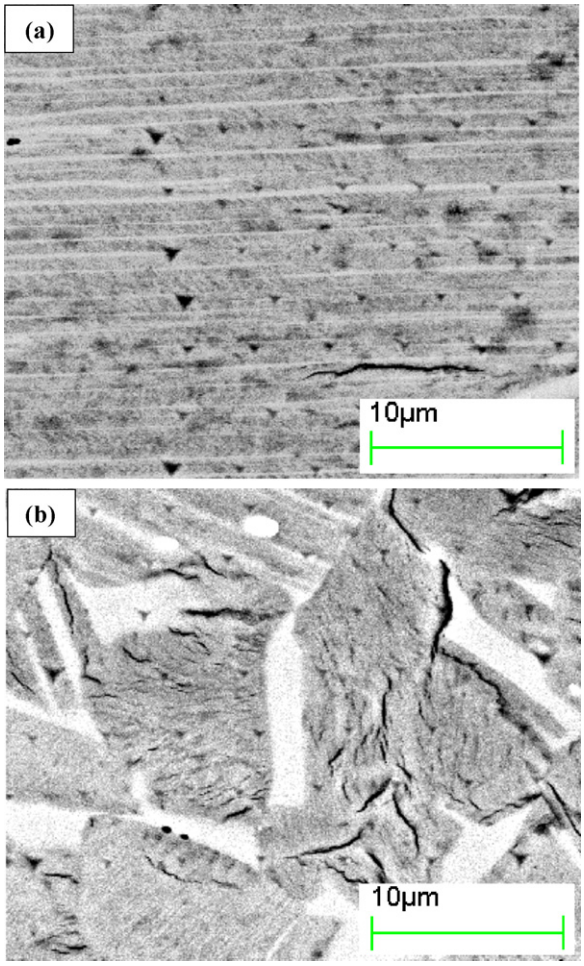

Fig. 6. Scanning electron micrographs (BSE mode) showing microstructure and also arrays of indents (a) on lamellar colony and (b) on equiaxed grains of mechanically polished Ti–46Al–8Nb alloy.

of the surface hardening during dry sliding was observed as a dramatic decrease of the wear rate at a constant load for the steels of various carbon contents, and this was attributed to the phase change in the surface layer [36].

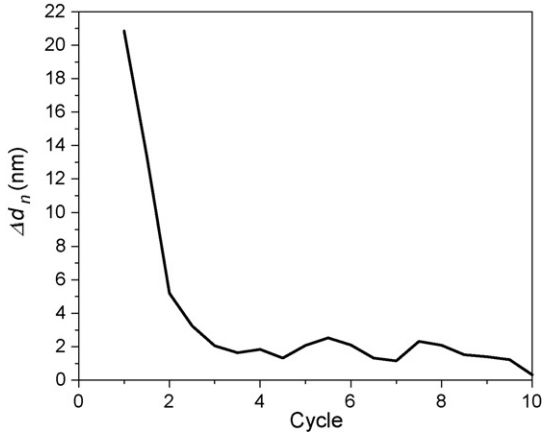

Fig. 7. Dependence of the difference of the normal tip displacement Δd_n on the number of cycles during scratch test performed at constant normal force of 500 μN on electrolytically polished Ti–46Al–8Nb alloy.

4. Conclusions

Considering the importance of surface hardness on the wear behavior of a tribo-mechanical system in sliding, indentation experiments have been carried out to investigate the strengthening of the TiAl(Nb) alloys during mechanical polishing, which can be considered as a friction process. During mechanical polishing the surfaces of both the Ti–46Al–8Nb and Ti–46Al–8Nb–0.2C alloys get work hardened. The work hardening is more pronounced for the Ti–46Al–8Nb alloy, even though the Ti–46Al–8Nb alloy is generally suffering from lower ductility as compared to the Ti–46Al–8Nb–0.2C alloy. This has been attributed to the presence of carbon.

The cold working (hardening) preferentially take place in the γ phase during the mechanical polishing, probably due to "self-stopping" of the twinning process. The overall mechanical hardening of these materials is mainly due to the hardening of the γ phase. In this case, the twinning also causes the opening of the brittle micro-cracks on the sample surface. When the mechanically hardened layer is removed by electrolytic polishing, the hexagonal α_2 phase is found to be harder than the tetragonal γ phase.

Furthermore, it is demonstrated that for the electrolytic polished samples the average hardness of the lamellar colonies is higher than that of the equiaxed grains. However, in the case of the mechanically polished alloys, the hardness of both structural features is found to be similar and could be explained by the preferential hardening of the γ phase during mechanical polishing. Additionally, the effect of the surface roughness on the measured hardness cannot be excluded. Scratch tests also shed light on the mechanical behavior of these alloys, illustrating a clear hardening effect at the near-surface region during the cyclic lateral tip movement.

Acknowledgements

Financial support received from the European Space Agency and the European Commisssion through the IMPRESS project (EU 6th Framework Program under contact number NMP3-CT-2004-500635) is gratefully acknowledged. The authors are grateful to Dr. Ulrike Hecht and her colleagues at ACCESS (Aachen, Germany) for kindly providing the alloys studied here.

The authors are also grateful to Dr. Arnaud Caron for the measurements of Poisson's ratio performed at the Abteilung Physikalische Grundlage, Frauenhofer Institut für Zerstörungsfreier Prüfung, Universität des Saarlandes. The authors would also like to thank Mr. Alexander Minkow at Ulm University for the assistance in the SEM measurements.

References

[1] L. Cao, H.W. Wang, C.M. Zou, Z.J. Wei, J. Alloys Compd. 484 (2009) 816–821.
[2] Y.H. Wang, J.P. Lin, Y.H. He, X. Lu, Y.L. Wang, G.L. Chen, J. Alloys Compd. 461 (2008) 367–372.
[3] F. Yang, F.T. Kong, Y.Y. Chen, S.L. Xiao, J. Alloys Compd. 496 (2010) 462–466.
[4] J. Fan, X. Li, Y. Su, J. Guo, H. Fu, J. Alloys Compd., doi:10.1016/j.jallcom.2010.07.122.
[5] H.B. Yu, D.L. Zhang, Y.Y. Chen, P. Cao, B. Gabbitas, J. Alloys Compd. 474 (2009) 105–112.
[6] H.P. Qu, P. Li, S.Q. Zhang, A. Li, H.M. Wang, Mater. Des. 31 (2010) 574–582.
[7] Y. Hong, Y.-C. Wu, Y. Li, F.-T. Wang, Q.-P. Wang, D.-H. Li, J. Aeronaut. Mater. 29 (2009) 17–20.
[8] S.-L. Xiao, J. Tian, L.-J. Xu, Y.-Y. Chen, H.-B. Yu, J.-C. Han, Trans. Nonferrous Met. Soc. China 19 (2009) 1423–1427.
[9] J. Lapin, Z. Gabalcova, O. Bajana, Metall. Mater. 47 (2009) 154–162.
[10] H. Zhang, X. He, X. Qu, L. Zhao, Mater. Sci. Eng. A 526 (2009) 31–37.
[11] T.-T. Ai, Front. Mater. Sci. China 2 (2008) 330–333.
[12] J.Y. Jung, J.K. Park, Scripta Mater. 34 (1996) 1581–1587.
[13] F. Appel, M. Oehring, W. Wagner, Intermetallics 8 (2000) 1283–1312.
[14] S. Gebhard, F. Pyczak, M. Goumlken, Mater. Sci. Eng. A 523 (2009) 235–241.
[15] M. Göken, M. Kempf, W.D. Nix, Acta Mater. 49 (2001) 903–911.

[16] M. Kempf, M. Göken, H. Vehoff, Mater. Sci. Eng. A 329–331 (2002) 184–189.
[17] X.-P. Liu, W.-H. Tian, C.-L. Guo, Z.-Y. He, Z. Xu, Trans. Nonferrous Met. Soc. China 16 (2006) s2026–s2029.
[18] J. Xia, C.X. Li, H. Dong, T. Bell, Surf. Coat. Technol. 200 (2006) 4755–4762.
[19] D. Roy, B. Basu, A. Basu Mallik, Intermetallics 13 (2005) 733–740.
[20] M. Masmoudi, M. Assoul, M. Wery, R. Abdelhedi, F. El Halouani, G. Monteil, J. Alloys Compd. 478 (2009) 726–730.
[21] H. Czichos, Tribology—A System Approach to the Science and Technology of Friction, Lubrication and Wear, Tribology Series 1, Elsevier Science Publishers B.V., Netherlands, 1978.
[22] S.A. Kouhanjani, A. Zare-Bidaki, M. Abedini, N. Parvin, J. Alloys Compd. 480 (2009) 505–509.
[23] F.P. Bowden, D. Tabor, The Friction and Lubrication of Solids, Oxford Univ. Press, New York, 2001.
[24] K. Durst, B. Backes, M. Göken, Scripta Mater. 52 (2005) 1093–1097.
[25] L. Wagner, J.K. Bigoney, in: C. Leyens, M. Peters (Eds.), Titanium and Titanium Alloys, Wiley-VCH, 2003.
[26] W.C. Oliver, G.M. Pharr, J. Mater. Res. 7 (1992) 1564–1583.
[27] F. Appel, M. Oehring, in: C. Leyens, M. Peters (Eds.), Titanium and Titanium Alloys, Wiley-VCH, 2003.
[28] L. Berger, Mechanische Charakterisierung nanostrukturierter Funktionsschichten durch Indentations- und Scratching-Verfahren, Dissertation, 2001.
[29] J.B. Pethica, W.C. Oliver, Mater. Res. Soc. Symp. Proc. 130 (1989) 13–23.
[30] N. Deyneka-Dupriez, U. Herr, H.-J. Fecht, A. Pfrang, Th. Schimmel, B. Reznik, D. Gerthsen, J. Mater. Res. 23 (2008) 2749–2756.
[31] V.M. Imayev, R.M. Imayev, G.A. Salischev, K.B. Povarova, M.R. Shagiev, A.V. Kuznetsov, Scripta Mater. 36 (1997) 891–897.
[32] X. Wu, D. Hu, M. Preuss, P.J. Withers, M.H. Loretto, Intermetallics 12 (2004) 281–287.
[33] T.R. Bieler, A. Fallahi, B.C. Ng, D. Kumar, M.A. Crimp, B.A. Simkin, A. Zamiri, F. Pourboghrat, D.E. Mason, Intermetallics 13 (2005) 979–984.
[34] C. Mercer, W.O. Soboyejo, Scripta Mater. 35 (1996) 17–22.
[35] M.S. Bobji, S.K. Biswas, Tribol. Lett. 7 (1999) 51–56.
[36] N.C. Welsh, Philos. Trans. R. Soc. Lond. A 1077 (1965) 31–70.